Hydrol. Earth Syst. Sci. Discuss., 8, 6155–6197, 2011
www.hydrol-earth-syst-sci-discuss.net/8/6155/2011/
doi:10.5194/hessd-8-6155-2011

Hydrology and Earth System Sciences Discussions

Sand box experiments to evaluate the influence of subsurface temperature probe design on temperature based water flux calculation

M. Munz[1,2], **S. E. Oswald**[1], **and C. Schmidt**[2]

[1]Institute of Earth and Environmental Science, University of Potsdam, 14476 Potsdam, Germany
[2]Department of Hydrogeology, Helmholtz Centre for Environmental Research – UFZ, 04318 Leipzig, Germany

Received: 27 May 2011 – Accepted: 8 June 2011 – Published: 24 June 2011

Correspondence to: M. Munz (munz@uni-potsdam.de)

Published by Copernicus Publications on behalf of the European Geosciences Union.

Abstract

Quantification of subsurface water fluxes based on the one dimensional solution to the heat transport equation depends on the accuracy of measured subsurface temperatures. The influence of temperature probe setup on the accuracy of vertical water flux calculation was systematically evaluated in this experimental study. Four temperature probe setups were installed into a sand box experiment to measure temporal highly resolved vertical temperature profiles under controlled water fluxes in the range of $\pm 1.3\,\mathrm{m\,d^{-1}}$. Pass band filtered time series provided amplitude and phase of the diurnal temperature signal varying with depth depending on water flux. Amplitude ratios of setups directly installed into the saturated sediment significantly varied with sand box hydraulic gradients. Amplitude ratios provided an accurate basis for the analytical calculation of water flow velocities, which matched measured flow velocities. Calculated flow velocities were sensitive to thermal properties of saturated sediment and to probe distance, but insensitive to thermal dispersivity equal to solute dispersivity. Amplitude ratios of temperature probe setups indirectly installed into piezometer pipes were influenced by thermal exchange processes within the pipes and significantly varied with water flux direction only. Temperature time lags of small probe distances of all setups were found to be insensitive to vertical water flux.

1 Introduction

Understanding surface water-groundwater exchange flux is of prime importance for understanding saturated sediment biogeochemistry and hydroecology (Krause et al., 2011; Sophocleous, 2002; Boulton et al., 1998). Several direct and indirect measurement methods where applied during field experiments to quantify these surface water groundwater exchange flux (Kalbus et al., 2006; Rosenberry and LaBaugh, 2008). A promising experimental approach is the use of natural heat as a tracer. The occurrence of heat in shallow hydrologic river-aquifer systems and its continuous exchange

HESSD
8, 6155–6197, 2011

between surface water, underlying streambed sediments and adjacent groundwater, result in temperature profiles or subsurface temperature variations that can be measured and used for quantifying the water exchange flux (Anderson, 2005; Constantz, 2008). Various analytical solutions have been developed to solve the 1-D heat transport equation (Suzuki, 1960; Stallman, 1965; Bredehoeft and Papadopolus, 1965; Turcotte and Schubert, 1982; Silliman et al., 1995). Specific to field data availability and analytical solutions data requirements, they were applied in several case studies to evaluate temperature profiles (e.g. Constantz et al., 2003; Schmidt et al., 2006, 2007) or temperature time series (e.g. Keery et al., 2007; Hatch et al., 2006; Rau et al., 2010). Time series methods that determine streambed flux, are based on the quantification of changes in amplitude (amplitude ratio) and phase shift (time lag) between pairs of subsurface temperature time series. Amplitude and phase information of temperature time series can be derived by pass band filtering (Hatch et al., 2006) or dynamic harmonic regression (Keery et al., 2007) signal processing techniques, both, enabling fast data processing and fast analytical evaluation. Lautz (2010) tested impacts on analytical flux estimates for the case of violated boundary conditions using numerical simulation. She found the greatest source of error to be due to non-vertical flow in the streambed. Schornberg et al. (2010) assessed the error introduced to the analytical solution provided by Bredehoeft and Papadopolus (1965), which is for the assumption of a heterogenous saturated sediment showing a pronounced contrast between hydraulic conductivities. The results of their simulations indicate that the method fails to provide reliable discharge estimates. Rau et al. (2010) evaluated measured temperature time series of three Australian rivers using two different analytical solutions and demonstrated inconsistencies in flux results between both methods. Jensen and Engesgaard (2011) compared Darcian flow velocities derived by time series analysis with seepage meter measurements at the Holtum Stream (Denmark) and found noticeable differences in mean flux values and ranges. Applying heat as a tracer is not only limited by inaccuracies of data evaluation, but also by practical limitations such as the accurate measurement of subsurface temperatures. This experimental study systematically compares the influence of temperature probe setup on amplitude ratio and time lag, and on the overall accuracy of the analytical water flux calculation of several direct and indirect temperature probe installations. The objectives are to evaluate the potential of temperature amplitude ratio and time lag to be used as targets for analytical flux calculation over a wide range of upward and downward fluxes; to show differences between amplitude ratios and time lags of common and new developed direct and indirect temperature probe setups; and to asses the overall accuracy of the flux calculation depending on temperature probe setup. Therefore, temperature time series of a long term sand box experiment were measured at multiple depths under controlled flux conditions ranging from $-1.30\,\mathrm{m\,d^{-1}}$ (downward) to $1.29\,\mathrm{m\,d^{-1}}$ (upward). Temperature probes were directly installed into the sediment by lost cone drilling, using a newly developed Multi Level Temperature Stick and, indirectly, inserting the temperature probes into a bottom screened and a complete screened piezometer pipe. Measured temperatures were analysed using established time series methods (Keery et al., 2007; Hatch et al., 2006).

2 Methods

2.1 Heat transport theory and data analyses

Temperature time series of the surface water contain components of various frequencies. These components can be classified into cyclic variations caused by solar radiation, and into random variations caused by short term disturbances of the radiative flux by shading of clouds, vegetation or heat introduced by precipitation into the system (Sinokrot and Stefan, 1993). As the variation of solar radiation has a daily and annual behaviour, there are theoretically two strong sinusoidal cyclic components in the temperature time series of frequencies, of one cycle per day and one cycle per year (Keery et al., 2007). The naturally introduced surface water temperature signal propagates into the sediment. Thereby the signal is reduced in amplitude and shifted in time depending on the thermal properties of the streambed and actual surface water-groundwater exchange fluxes (Constantz and Stonestrom, 2003; Keery et al., 2007; Hatch et al., 2006; Rau et al., 2010).

Stallman (1965) developed a complete analytical solution that simultaneously describes the heat transport by conduction and heat transport by advection (convection) for steady water flow. For this, he assumed a sinusoidal temperature oscillation of constant amplitude at the surface-subsurface interface and a constant temperature at infinite depth. This approach can be used to determine constant and uniform infiltration rates or exchange fluxes normal to the surface in a homogeneous medium.

Keery et al. (2007) reformulated this solution to compute an unknown vertical water flux (q) with given observations of oscillating temperatures at two depths below the surface. They derived one implicit formulation based on thermal properties of the system and amplitude attenuation (Eq. 1), and one explicit formulation based on thermal properties of the system and time lag (Eq. 2):

$$0 = \left(\frac{H^3 D}{4z}\right) q^3 - \left(\frac{5H^2 D^2}{4z^2}\right) q^2 + \left(\frac{2HD^3}{z^3}\right) q + \left(\frac{\pi c \rho}{\lambda_0 \tau}\right)^2 - \frac{D^4}{z^4} \quad (1)$$

where

$$D = \ln\left(\frac{A_{z+\Delta z,t+\Delta t}}{A_{z,t}}\right) \quad \text{and} \quad H = \frac{c_w \rho_w}{\lambda_0}.$$

$\frac{A_{z+\Delta z,t+\Delta t}}{A_{z,t}}$ is the amplitude ratio of the amplitude of a single frequency oscillation at depth $z+\Delta z$ and time $t+\Delta t$ and at depth z (m) and time t (s), respectively. τ is the time period (s) of that frequency, ρ is the density of saturated sediment, ρ_w is the density of water (kg m^{-3}), c is the specific heat capacity of the saturated sediment, c_w is the specific heat capacity of water (J kg^{-1} K^{-1}) and λ_0 is the baseline thermal conductivity of the saturated sediment (W m^{-1} K^{-1}).

HESSD
8, 6155–6197, 2011

The explicit formulation is:

$$q = \left(\frac{c^2 \rho^2 z^2}{\Delta t^2 c_w^2 \rho_w^2} - \frac{16\pi^2 \Delta t^2 \lambda_0^2}{\tau^2 z^2 c_w^2 \rho_w^2} \right)^{\frac{1}{2}} \quad (2)$$

where Δt is the time lag between time of amplitude at $z + \Delta z$ and time of amplitude at z, Δz is the vertical distance between two vertical measurement points. The resulting flux of Eq. (1) is positive in downward and negative in upward direction, while Eq. (2) does not allow distinguishing between flux directions.

To satisfy the upper boundary condition of the analytical solution, the most pronounced temperature frequency of one cycle per day was isolated of the temperature time series by a pass band filter with a Kaiser window. The filter was set to a pass band frequency range of 0.9 d^{-1} to 1.1 d^{-1} and to stop band frequencies of <0.6 d^{-1} and >1.4 d^{-1} as suggested by Hatch et al. (2006). To avoid edge effects, the first and the last seven days of data were used to extent the measured temperature time series. Finally, a peak detection routine was applied to the filtered time series to detect daily maxima (amplitude) and their exact timing. The results were plotted and checked visually for completeness of corresponding peaks. Daily amplitudes and timings were used to calculate amplitude ratios and phase shifts, which were used to calculate vertical sand box water flow velocities based on Eqs. (1) and (2).

To compare the amplitude ratios and time lags for each hydraulic head difference (Δh), the non-parametric measures median and 95 % confidence interval of the median were used. It was visually checked whether or not the 95 % confidence intervals of each median overlap. In case they do not overlap, the amplitude ratios and the time lags occurring for each Δh are seen as significantly different from each other at the 5 % significance level and are regarded to be sensitive to water flux. Based on this amplitude ratio and time lag sensitivity to different magnitudes of water flux, we evaluated whether subsurface temperature patterns provide a sufficient basis for analytical, temperature-based water flux calculations.

HESSD
8, 6155–6197, 2011

To characterize experimental water fluxes in terms of dominant heat transport mechanism and thermal stability the dimensionless Peclet and Rayleigh number of energy transport have been applied. The Peclet number is the ratio of energy transported by advection to the energy transported by conduction (Domenico and Schwartz, 1990). Peclet numbers greater than one indicate that advective heat transport dominates over conductive heat transport. The Rayleigh number is the ratio of energy transported by free convection to the energy transported by conduction (Domenico and Schwartz, 1990). Free convection occurs when fluid flow is forced by buoyancy due to density differences where a dense fluid overlies a less dense one; caused by temperature or solute concentration gradients.

2.2 Experimental setup

The model apparatus consists of a polyvinylchloride barrel with a diameter of 0.68 m and a total height of 0.80 m. To create barrel in and outlets two $\frac{3}{4}$ inch openings were drilled at 0.04 m and 0.7 m above the bottom. At 0.08 m above the bottom in/outlet a stainless steel frame covered with stainless steel gauze was exactly fitted in the barrel and sealed with silicon on its sides. Above that frame, the barrel was filled with a 0.5 m thick homogeneous, medium-grained quartz sand layer. The dry sand was slowly trickled into the barrel and was stirred from time to time to assure a homogeneous sediment distribution as good as possible. The barrel was buried into the ground to the height of the sediment surface at a sun-exposed position at an experimental field site at the Helmholtz Centre for Environmental Research – UFZ in the city of Leipzig, Germany (Fig. 1). Consequently, the buried part of the barrel was in thermal contact with the natural ground sediment and thus with the natural thermal regime. The non-buried part was in thermal contact with the atmosphere.

A conventional 10 l bucket, with two $\frac{3}{4}$ inch openings built in, one below the top and one above the bottom of the bucket, was used as vertically adjustable water reservoir to control the vertical hydraulic gradient. The bucket's bottom opening and the barrel's bottom in/outlet were connected via a $\frac{3}{4}$ inch ordinary garden tube. The barrel sediment

HESSD
8, 6155–6197, 2011

was slowly saturated with water supplied through the barrel bottom inlet. In total 58 l were necessary to saturate the sediment.

Vertical water fluxes were generated by adjusting the absolute high of the bucket to create hydraulic head differences (Δh) from −0.026 m to 0.026 m in 8 steps. Negative gradients, i.e. water level of barrel was higher than water level of bucket, generated vertical downward flux through the sediment. Therefore water was introduced into the top of the barrel, filtrated through the sediment and left the system through the upper bucket opening. The water supply was adjusted to enable a minor water volume discharge through the barrel top outlet avoiding large water level fluctuations. In contrast, positive gradients, i.e. if the water level of the barrel was lower than the water level of the bucket, generated a vertical upward flux. Upward fluxes were induced by introducing water into the top of the bucket which flowed through the sediment body and left the system through the barrel top outlet. Again the water supply was adjusted in a way to enable water discharge through the upper bucket opening avoiding large water level and temperature fluctuations within the bucket.

The experiment was run from June to October 2010. Each hydraulic gradient was sustained for at least 7 days. System discharge was measured periodically (in general three times per day) using containers with control volumes from one to ten litre. For these measured discharges the average daily discharge (q) was calculated. All q of constant hydraulic gradients were averaged to the gradient dependent flux ($\overline{q}$). The 95 % confidence intervals of $\overline{q}$ were calculated and used to test whether the fluxes were significantly different between the different hydraulic gradients.

In order to determine hydraulic and hydromechanic sediment properties a conservative salt tracer experiment was conducted under a downward flow condition. The tracer was initiated as step pulse injection to the upper barrel water reservoir. Initial concentration at the upper barrel water reservoir was 0.60 g l^{-1} which was below the estimated threshold concentration for the onset of free convection (0.66 g l^{-1}). The measured discharge and arrival time of maximal tracer concentration were used to calculate the effective porosity and saturated hydraulic conductivity based on Darcy's law.

An initial estimate of the total porosity (n) was derived by the water volume needed to saturate the sediment of known volume. The sediment solutes dispersivity was derived by analyses of the statistical temporal moments of the tracer break through curves (Cirpka and Kitanidis, 2000, 2001).

2.3 Temperature probe installation

The sand box was instrumented at a depth of 0.015 m, 0.065 m, 0.165 m and 0.365 m below the sediment surface with temperature probes using the setups described in the following.

1. Vertical installation of TidbiTs within the sediment (Sediment Probes)

   The TidbiT v2 temperature logger (Onset computer cooperation, Pocasset, Massachusetts, US) contains a thermistor integrated with signal-conditioning circuitry, a real time clock and a memory unit. The constituent parts are inserted in a 3 cm × 1.7 cm large epoxy case which is waterproof up to 305 m depth. The measurement accuracy is 0.2 °C over a range from 0 to 50 °C. The logger resolution is 0.02 °C with a response time of 5 min in water.

   The TidbiT temperature loggers were connected via a thin fibre at predefined intervals and fixed to a steel cone. The cone was loosely fitted to a steel pipe with an inside diameter of 0.04 m and a length of 1.50 m. The pipe was driven into the barrel sediment using a sledge hammer. A metal rod was inserted down the pipe and pushed to detach the cone from the metal pipe while the pipe was slowly removed (lost cone drilling). The fibre with the connected TidbiTs was held tight all the time to ensure the loggers being in the right position while the sediment was collapsing. Thus, the temperature loggers are directly in thermal contact with sediment.

2. Installation of the Multi Level Temperature Stick (MLTS)

HESSD
8, 6155–6197, 2011

The Multi Level Temperature Stick (Umwelt und Ingenieurtechnik GmbH, Dresden, Germany) is a polyoxymethylene stick (total length of 0.657 m and a diameter of 0.02 m) with eight integrated temperature sensors. The thermal contact of the sensors to the surrounding material is ensured through thin stainless steel flat blanks. The temperature is measured with each sensor simultaneously with an accuracy of 0.07 °C over a range from 5 to 45 °C. The logger resolution is 0.04 °C. The MLTS was pushed into the sediment to a depth of 0.4 m, so that the four deepest probes are inside the sediment and two probes log the surface water temperature.

3. Vertical installation of TidbiTs inside a bottom screened piezometer (PBS)

   The high density poly ethylene (HDPE) piezometers with a connected HDPE drive point were driven vertically into the sediment. The total length of the piezometer is 1.50 m with an inner diameter of 0.05 m. The piezometer was screened 0.06 m above the drive point over a section of 0.03 m, in a total depth between 0.34–0.37 m. The small screen keeps the piezometer filled with water, to enable a good thermal contact between the sensor and the sediment. To screen the piezometers the pipes were screwed at three sides with a thin sawing blade (0.05 mm) in regular distances of 5 mm. The distance between drive point and beginning of the screen allows little sediment particles to settle down inside the piezometer without clogging the screen. The TidbiT temperature loggers were connected via a thin fibre at predefined intervals. This logger chain was suspended within the piezometer.

4. Vertical installation of TidbiTs inside a complete screened piezometer (PCS)

   The installation of the PCS is the same as described for the PBS except the piezometer pipe which was screened 0.06 m above the drive point over a section of 0.36 m, in a total depth from 0.01 to 0.37 m. The complete screen allows barrier free heat propagation between the temperature sensors and the sediment with negligible influence of the piezometer material. Because of the limited number of

HESSD
8, 6155–6197, 2011

temperature loggers available, the TidbiT logger chain (cp. setup 3) was switched between the PBS and PCS after half of the time of equal hydraulic gradient. To check thermal regime of the other pipe respectively, one TidbiT temperature logger was suspended within the piezometer at a depth of 0.165 m (single piezometer logger).

All data loggers were calibrated in the upper water reservoir of the barrel during five days. For these data, correction factors were established by linear regression of each logger with a reference logger. All temperature loggers were set to a 15 min measurement interval.

The previously described Sediment Probe and PBS setups were chosen for installation as they are the most common to install temperature probes within saturated sediment. The Sediment Probes were embedded directly within the sediment. The time to reach the thermal equilibration between the temperature probe and saturated sediment is supposed to be less than the monitoring interval of 15 min. Therefore the Sediment Probe setup was assumed to be the least intrusive setup and that it was in best thermal contact with the saturated sediment. The PBS temperature probes were separated from the saturated sediment by ideally non-moving water and by the piezometer side wall. To potentially reduce the effect of piezometer side wall the PCS setup was designed as a modification of the PBS setup. The MLTS was used as it is a newly developed probe design characterized by good practical application in terms of installation, known accurate probe spacing and data availability during operation. The MLTS probes were embedded in a HDPE rod separated by small stainless steel plates from the saturated sediment.

Each profile probe setup, having four temperature probes recording the sediment temperatures, allows calculation of amplitude ratio and phase shift relations for six probe pairs. All probe combinations of all installations were evaluated with respect to the sensitivity of their amplitude ratios and time lags to variations of Δh. For brevity only the results of probe pairs which cover minimum ($\text{pair}_{0.065-0.015}$), intermediate ($\text{pair}_{0.165-0.065}$) and maximum probe distances ($\text{pair}_{0.365-0.015}$) are discussed

HESSD
8, 6155–6197, 2011

(subscript specifies depth of installation of used temperature probes). However, they provide a sufficient overview on the experimental results as all other probe pairs overlap, i.e. use equal temperature probes but integrate over different segments of the sand box, and are therefore potentially redundant.

2.4 Estimation of saturated sediment thermal properties and sensitivity analysis

The calculated vertical flow velocities depend on observed amplitude ratio or time lag and on thermal properties of the saturated sediment. Thus thermal properties have to be determined for input into Eqs. (1) and (2). As thermal properties are difficult to measure outside the laboratory (Stonestrom and Blasch, 2003), we used literature based values which were additionally calibrated during no-flow conditions.

Heat capacities of porous materials depend on their composition and bulk density (Stonestrom and Blasch, 2003). Thus the volumetric heat capacity of the barrel sediment was calculated from the volume-weighted sum of density and the volume-weighted sum of heat capacities of constituents making up the saturated sediment based on experimental estimated total porosity. The thermal conductivity of porous materials depends upon the composition and arrangement of the solid phase. Due to the complexities of pore geometry, this dependence is non-linear and difficult to predict (Wierenga et al., 1969). As a first assumption, the thermal conductivity of saturated sediment was calculated from the volume-weighted sum of thermal conductivities of constituents making up the saturated sediment. The literature based, averaged thermal conductivity was calibrated by least square minimisation between calculated flow velocities and zero. We restricted the calibration to a no-flow condition as there will be no uncertainties due to experimentally measured water flux and thus calibration of thermal parameter will be unaffected of these experimental uncertainties. Calibrated thermal properties were used for all flux calculations.

The accuracy of flow velocity calculation depends on the set of thermal sand box parameter and accurate measurement of temperature. To evaluate the parameter-based sensitivity of calculated flow velocities we assessed a sensitivity analysis of Keery's analytical solution (Eq. 1) comprising the most uncertain state variables: volumetric heat capacity, thermal conductivity of saturated sediment and assumed spacing between temperature probes. Therefore parameter values were systematically varied using a minimum and a maximum deviation of 50 % of the optimum parameter. The impact of altered parameter values on the model was assessed by absolute changes of flow velocity.

2.5 Impact of thermal dispersivity on vertical sand box water flow velocities

Since there is an ongoing discussion about the effects of thermal dispersion on vertical flow velocities (Keery et al., 2007; Hatch et al., 2006), we also quantified the sensitivity of flow velocity to thermal dispersion. In our analysis, thermal dispersion is treated in analogy to the solute dispersion. The thermal dispersion (D_{th}) is the sum of the bulk soil thermal conductivity with stationary fluids and a kinematic thermal dispersion term, resulting from the heterogeneity of water velocities within and between water-filled sediment pores. To account for the two processes, D_{th} is defined as (Anderson, 2005):

$$D_{th} = \frac{\lambda_e}{c\rho} = \frac{\lambda_0}{c\rho} + \alpha_{th} \times |q| \quad (3)$$

where λ_e is the effective thermal conductivity of the saturated sediment ($\mathrm{W\,m^{-1}\,K^{-1}}$), λ_0 is the baseline thermal conductivity in absence of fluid flow ($\mathrm{W\,m^{-1}\,K^{-1}}$) and α_{th} is the thermal dispersivity (m). Some researchers argue that values of thermal dispersion are comparable to those of conservative solute dispersion (de Marsily, 1986; Hopmans et al., 2002) while others conclude that the effect of thermal dispersion ($\alpha_{th} \times |q|$) is negligible compared to the baseline thermal diffusivity (Bear, 1972; Ingebritsen and Sanford, 1998). Thus, to test the sensitivity of calculated flow velocity to thermal dispersion we assuemed the thermal dispersivity to be in the range of solute dispersivities observed by the solute tracer experiment.

HESSD
8, 6155–6197, 2011

To solve the 1-D heat transport equation by means of an analytical solution including convective, conductive and dispersive heat transport, we used the solution presented by Hatch et al. (2006). Their analytical solution is based on the same assumptions and boundary conditions as the Keery et al. (2007) solution. The main difference is that Hatch et al. (2006) defined the effective thermal diffusivity analogous to Eq. (3), while Keery et al. (2007) set the effective thermal diffusivity equal to the baseline thermal diffusivity.

3 Results and discussion

3.1 Experimental flux

The averaged, gradient-dependent water fluxes in the sand box and their 95 % confidence intervals are given in Table (1). Ideally one would expect constant discharges as long as Δh is kept constant. However, we observed variations of q during constant Δh which were caused by the temperature dependency of hydraulic conductivity as well as by disturbances of the experiment during operation. Such disturbances mainly occurred at barrel and bucket outlets where slugs and polls caused time dependent Δh variations up to 0.002 m; but variations of q during constant Δh condition remained small compared to differences between $\overline{q}$. Differences between $\overline{q}$ were significant on the basis of the 5 % confidence interval except for $\overline{q}$ of $\Delta h = 0.008$ m and $\Delta h = 0.013$ m. The average discharges ranged between $-1.30\,\mathrm{m\,d^{-1}}$ to $1.29\,\mathrm{m\,d^{-1}}$ (Table 1) and therewith agree well with water fluxes typically observed in natural surface water-groundwater systems (Conant, 2004).

The ratio of convective to conductive heat transport varied in dependence of Δh. Experimental flux conditions were dominated by forced convective heat transport also for $\Delta h = 0.002$ m (Table 1). Only for $\Delta h = 0$ convective heat transport did not occur and the system was driven by pure heat conduction. Rayleigh numbers (Table 1) less than the critical Rayleigh number of $4\pi^2$ (Lapwood, 1948; Bear, 1972) indicate that

HESSD
8, 6155–6197, 2011

measured temperature gradients were too small to cause substantial instabilities of thermal flow regime. Thus, a 1-D conductive-convective heat transport model can accurately describe the experimental thermal regime.

3.2 Relations of amplitude ratio and time lag of Sediment Probes to hydraulic head differences

The Sediment Probe setup was used to analyse the behaviour of amplitude ratios and time lags in relation to specified Δh because this setup was assumed to be the least intrusive setup and to be in best thermal contact with the saturated sediment.

Figure 2 shows daily amplitude ratio distributions of Sediment Probes of selected probe pairs depending on Δh. The overall range of amplitude ratios was between 0 (completely damped) and 1 (no damping) and illustrates the damping of amplitudes while heat propagates through saturated sediment. Amplitude ratios decreased with increasing Δh and increasing probe spacing (Fig. 2). Thus amplitude ratios were dependent on hydraulic conditions and monitoring depth.

The probe pair$_{0.065\text{–}0.015}$ showed significant differences between the amplitude ratios of all Δh with exception of the pair wise comparison of $\Delta h = 0.008$ m and $\Delta h = 0.013$ m (Fig. 2a); accurately reflecting differences between $\overline{q}$.

The intermediate probe pair$_{0.165\text{–}0.065}$ indicated significant differences from $\Delta h = -0.026$ m up to $\Delta h = 0.008$ m (Fig. 2b) and the deep probe pair$_{0.365\text{–}0.015}$ indicated significant differences from $\Delta h = -0.026$ m up to $\Delta h = 0.002$ m only (Fig. 2c). There was a lack of significance, during high upward fluxes evoked by violations of assumed constant temperature at the bottom of the sandbox. The deep and intermediate temperature probes at 0.365 m and 0.165 m depth partly revealed temperature variations which were not caused by the diurnal surface temperature signal. Furthermore, oscillating tap water temperatures at the bottom of the sand box influenced the deep temperature probes. With increasing upward fluxes, the effect of variable water temperatures at the bottom inlet became more pronounced. This constrained the validity of analytical solution for $\Delta h = 0.013$ m and 0.026 m when probe pairs with deep temperature probes were used. Sensors close to the sediment surface and separated by small distances, like the probe $\text{pair}_{0.065-0.015}$ were not capable of resolving higher downward fluxes ($\Delta h < -0.026$ m) because the amplitude ratios were not significantly different from unity (Fig. 2a).

In a similar manner as the temperature time signal was reduced in amplitude it was also shifted in time. The main difference of time shift compared to amplitude ratio is that it is only dependent on flux magnitudes but independent of the flux direction (Eq. 2). Hence, water fluxes of the same magnitude but different direction will result in identical time lags. The results for probe $\text{pair}_{0.065-0.015}$ (Fig. 3a) confirmed these theoretical relations. Here time lags between $\Delta h = -0.002$ and $\Delta h = 0.002$ as well as time lags between $\Delta h = -0.008$ m and $\Delta h = 0.008$ m were found to be similar. In contrast, time lags of probe $\text{pair}_{0.365-0.015}$ and probe $\text{pair}_{0.165-0.065}$ did not confirm the similarity of time lags for equal absolute hydraulic head differences.

The comparison between time lags of the same flux direction of the shallow probe $\text{pair}_{0.065-0.015}$ shows small, partly non-significant differences between Δh conditions. In contrast, time lags of the intermediate probe $\text{pair}_{0.165-0.065}$ differed significantly for all negative Δh. Time lags of the deep probe $\text{pair}_{0.365-0.015}$ differed significantly for Δh conditions from -0.026 m to 0.008 m compared to the average time lag of no-flow condition (Fig. 3). Thus, higher probe distances had higher time lags and were more significant to hydraulic head settings. Deviations of time lags of $\Delta h > 0.008$ m for all probe pairs were caused by variable temperatures at the bottom of the sand box.

In general, the time lags are less sensitive to Δh than the amplitude ratios. In turn, the time lags will remain sufficiently large to resolve high flow velocities up to $\pm 10\,\text{m}\,\text{d}^{-1}$ (Hatch et al., 2006). Hatch et al. (2006) developed theoretical type curves for amplitude ratio and phase shift as a function of flow rates for different streambed measurement spacing. Our experimental results are in agreement with the theoretical predictions at least for the tested flow range.

Success of quantifying exchange fluxes based on temperature measurements is dependent on the appropriate placement of temperature sensors. Decision of placement

HESSD
8, 6155–6197, 2011

depends on hydraulic and thermal properties of the sediment, surface water temperature amplitude and pore water velocities. Keery et al. (2007) monitored shallow sediment temperatures beneath the River Tern, Shropshire, England and found that temperatures recorded by sensors installed at 0.2 m and deeper showed very low diurnal temperature amplitudes. Fluxes observed at this site ranged from $-0.35\,\mathrm{m\,d^{-1}}$ to $0.48\,\mathrm{m\,d^{-1}}$. To test whether the temperature probes are located in the thermally active zone, preliminary calculations can be useful for selecting measurement depths and frequencies (Constantz et al., 2001). Critical evaluation of boundary conditions is essential to apply analytical solutions for vertical flux calculation. Also in natural systems, groundwater temperatures are not necessarily constant, especially in small, upland rivers characterized by shallow aquifers and which are strongly fed by groundwater. For this reason, the sources of subsurface temperature variability need to be considered for the correct interpretation of the obtained amplitude ratios and time lags.

All in all, the evaluation of the experimental data revealed that the Sediment Probe setup provided amplitude ratios sufficient to resolve sediment water fluxes of $-1.30\,\mathrm{m\,d^{-1}}$ to $1.29\,\mathrm{m\,d^{-1}}$ when daily amplitudes of 2 °C were present in the surface water. Large probe distances would be needed to resolve higher downward fluxes, as otherwise the observed amplitudes may not be sufficiently damped. Only the large temperature probe distance provided time lags, large enough to be sensitive to experimental fluxes for the given surface water amplitudes. Generally, sensors placed sufficiently close to the sediment surface to be influenced by the diurnal thermal signal had highest accuracy to resolve tested flux magnitudes by the amplitude ratio method.

3.3 Differences of amplitude ratio and time lag between temperature probe setups

In Sect. 3.2, the differences of amplitude ratios and time lags between Δh conditions of the Sediment Probe setup were analyzed. Based on these findings the general behaviour of amplitude ratios and time lags of Sediment Probes (Fig. 1, setup A) were compared to amplitude ratios and time lags of MLTS (B), PBS (C) and PCS

(D), respectively. Using amplitude ratios and time lags to compare these temperature probe setups the results will be uneffected by thermal skin effects, introducing additional time lags and dampening due to the material surrounding the temperature probe (Cardenas, 2010).

3.3.1 Sediment Probes vs. MLTS

The comparison of Sediment Probe and MLTS shows that the calculated daily amplitude ratios (RMSE = 0.01) and time lags (RMSE = 0.28) were in good agreement for both setups for a wide range of downward flow conditions (Fig. 4a). For upward flow conditions (positive Δh) we observed a slight underestimation of MLTS amplitude ratios (RMSE = 0.03) and a more obvious overestimation of MLTS time lags (RMSE = 0.45).

For downward flow conditions heat transport is dominated by advection. The thermal exchange between the fluid and MLTS was practically equal to thermal exchange between fluid and Sediment Probes yielding to comparable amplitude ratios and time lags. For upward flow conditions the direction of advection is directly opposed to heat conduction into the sediment.

Different thermal conductivities and heat capacities of sand and MLTS material potentially result in deviations of daily amplitude ratios and time lags between Sediment Probes and MLTS. The main material of MLTS is HDPE which is characterized by a higher volumetric heat capacity and lower heat conductivity than the quartz sand (Table 2). With higher volumetric heat capacity more energy is absorbed by the same material volume. Differences in heat capacities caused an increased damping of temperatures for MLTS compared to the true temperature signal occurring within the saturated sediment. The resulting MLTS amplitude ratios were lower than the Sediment Probe amplitude ratios (Fig. 4a).

Lower thermal conductivity caused an increased phase shift, e.g. the deep probes of MLTS reached their peak temperature later than true temperature signal occurring within the saturated sediment. Thus differences in thermal conductivity caused higher time lags of MLTS than of Sediment Probes (Fig. 4d). The deviations of the time lags

HESSD
8, 6155–6197, 2011

between Sediment Probe and MLTS setup were more pronounced than the deviations of amplitude ratios. This is because the thermal conductivity of HDPE is more than one order of magnitude lower than thermal conductivity of quartz whereby the heat capacity of HDPE is within the same order of magnitude as the heat capacity of quartz (Table 2).

Differences between Sediment Probes and MLTS only occurred when heat conduction became the dominant process of downward directed heat transport. Thereby deviations between temperature probe setups increased with depth of temperature probe installation, e.g. lowest deviations between amplitude ratios and time lags occurred for probe pairs located close to the surface. As the volumetric heat capacity of HDPE is only 11 % higher than the volumetric heat capacity of quartz sediment deviations in amplitude ratios between Sediment Probes and MLTS remained small, especially for probe $\text{pair}_{0.065-0.015}$ and $\text{pair}_{0.165-0.065}$. Thus, MLTS amplitude ratios of probe $\text{pair}_{0.065-0.015}$ and $\text{pair}_{0.165-0.065}$ can be used for appropriate estimation of vertical flow velocities. The MLTS setup is suitable to calculate water fluxes of at least $-1.30\,\text{m}\,\text{d}^{-1}$ to $1.29\,\text{m}\,\text{d}^{-1}$ providing that the temperature sensors are installed in the thermally active zone of the saturated sediment (e.g. probe $\text{pair}_{0.065-0.015}$). In contrast, the calculation of flow velocities using MLTS time lags was uncertain due to the general insensitivity of time lags to small flow velocities. As the magnitude of deviation between Sediment Probe and MLTS time lags was dependent on temperature probe distance it was not possible to establish a simple conversion factor to compensate setup dependent differences between Sediment Probes and MLTS.

The general differences of MLTS derived amplitude ratios for all Δh were comparable to the characteristics of Sediment Probe amplitude ratios. Also the MLTS setup could be used to significantly differ between Δh conditions from -0.026 m to 0.026 m as long as temperature probes installed within the sediment cover small distances of 0.05 m and high distances of 0.35 m.

HESSD
8, 6155–6197, 2011

3.3.2 Sediment Probes vs. PBS

The comparison of daily amplitude ratios based on Sediment Probes vs. PBS (Fig. 4b, e) reveals that most PBS amplitude ratios were higher (less damped) (RMSE = 0.09 °C) and time lags were shorter (RMSE = 1.1 h) than the corresponding Sediment Probe amplitude ratios and time lags. These deviations were caused by vertical thermal exchange processes occurring within the piezometer pipe independent of the saturated sediment thermal regime.

This might be caused by the onset of heat transport by free convection within the piezometer pipe. Maximal daily temperatures within the piezometer pipe vertically decreased. While shallow sediment temperatures decreased faster than deep sediment temperatures during nightly atmospheric cooling, temperatures of different PBS depth equilibrated (Fig. 5). We observed that at the point of time the temperatures of different observation depth reached equality, the temperatures started to decrease simultaneously until minimum atmospheric temperatures were reached (Fig. 5). Because of these effects minimum temperatures of PBC were nearly identical whereas Sediment Probe temperatures vertically increased with increasing depth. Resulting minimum temperatures at shallow PBS sensors (0.015 m and 0.065 m) were higher and temperatures at deep PBS sensors (0.165 m and 0.365 m) were lower than temperatures occurring within the saturated sediment (Fig. 5). In consequence temperature amplitudes at depth of 0.015 m and 0.065 m were lower and temperature amplitudes at depth of 0.165 m and 0.365 m were higher than corresponding sediment temperature amplitudes causing the general overestimation of Sediment Probe vs. PBS amplitude ratios (Fig. 4b).

Also the large underestimation of PBS time lags was a result of thermal exchange processes within the piezometer pipe. PBS temperature maxima of deep sensors (at 0.165 and 0.365 m) were reached earlier than maximum temperatures occurring within the saturated sediment (Fig. 5) causing lower time lags of PBS (Fig. 4e).

We also observed few PBS amplitude ratios that were lower and PBS time lags that were higher than the corresponding Sediment Probe amplitude ratios (Fig. 4b) and time lags (Fig. 4e). These deviations occurred when vertical thermal exchange processes within the piezometer pipe were absent. Thereby the measured temperatures at 0.015 m were constantly higher than measured temperatures at 0.065 m (stable thermal stratification). Such conditions were observed during experimental upward flow and low atmospheric temperature variations. For these experimental conditions, differences in heat capacities of PBS and saturated sediment caused an increased damping of PBS temperatures compared to the true temperature signal within the saturated sediment, yielding to lower amplitude ratios of the PBS (Fig. 4b). Higher time lags of PBS compared to Sediment Probes (Fig. 4e) were a result of lower thermal conductivity of water than of saturated sediment (Table 2). Thereby the induced temperature signal propagated slower into the ground within the piezometer pipe than within the saturated sediment.

3.3.3 Sediment Probes vs. PCS

The deviations between Sediment Probe and PCS amplitude ratios (RMSE = 0.11) and time lags (RMSE 1.2 h) were comparable to those between Sediment Probe and PBS (Fig. 4). Main differences between Sediment Probe and PCS occurred due to vertical thermal exchange processes within the complete screened piezometer pipe. For upward flow conditions, during stable thermal stratification, the differences between Sediment Probe and PCS were smaller and could be attributed to different thermal properties of temperature probe setups (cp. Sect. 3.3.2).

3.3.4 Sediment Probes vs. PCS and PBS

The similar behaviour of PCS and PBS was further confirmed by the concurrent measurements in both setups at 0.165 m depth. At this depth, PCS and PBS showed analogue temperature regimes. Differences between PBS and PCS setups were negligible compared to the differences between PBS/PCS and Sediment Probe setup. Thus the Piezometer Probe setups (PBS/PCS) will not be distinguished in the following chapters since their results and interpretations would be identical.

Vertical preferential flow along the piezometer pipes potentially influence the measured temperatures of PBS and PCS. Occurring preferential flow would result in less dampened amplitudes and faster signal propagation than observed for Sediment Probes. But as preferential flow would have been the reason causing these deviations, they would not have appeared for no-flow condition ($\Delta h = 0$). However, preferential flow causing the deviations between Sediment Probe and Piezometer Probe setups could be ruled out because we observed deviations between amplitude ratios (RMSE = 0.15) and time lags (RMSE = 2.3) for no-flow condition.

We highlighted the differences between temperature probe setups by comparing their amplitude ratios and time lags. Using these signal characteristics we could examine influences of thermal skin effects and uncertain thermal sediment characteristics. The smallest differences were found between Sediment Probes and MLTS setup. The differences between Sediment Probes and both, PBS and PCS were high. Hence, the use of Piezometer Probe amplitude ratios and time lags would cause substantial errors when they are used as targets to calculate vertical flow velocities.

3.4 Thermal properties of the sand box sediment

Calibrated baseline thermal diffusivity of the sand box sediment was found to be $1.19 \times 10^{-6}\,\mathrm{m^2\,s^{-1}}$. The corresponding heat capacity was $1870\,\mathrm{J\,kg^{-1}\,K^{-1}}$ and thermal conductivity was $4.75\,\mathrm{W\,m^{-1}\,K^{-1}}$. The calibration of thermal properties result in a wide range of parameter sets of heat capacity and thermal conductivity, having little RMSE, between calculated flow velocities and $q = 0$, in the range of 1×10^{-7} to $3 \times 10^{-7}\,\mathrm{m\,s^{-1}}$. All parameter sets of saturated heat capacity and thermal conductivity having the same saturated sediment dispersivity of $1.19 \times 10^{-6}\,\mathrm{m^2\,s^{-1}}$ (quotient of thermal conductivity and heat capacity) accurately described the heat transport behaviour under a no-flow condition.

HESSD
8, 6155–6197, 2011

Assuming a volumetric heat capacity of saturated sediment of 1870 $J\,m^{-3}\,K^{-1}$ (Table 2), the corresponding thermal conductivity was found to be 4.75 $W\,m^{-1}\,K^{-1}$, determined by minimum RMSE between calculated flow velocities and $q = 0$. The derived saturated thermal conductivity of the sand box sediment was higher than thermal conductivities of sediments commonly found in natural streambeds, which are in the range of 0.8 to 2.5 $W\,m^{-1}\,K^{-1}$ (Hopmans et al., 2002; Schön, 1998; Stonestrom and Blasch, 2003). This high thermal conductivity is the result of pure quartz sediment, which is highly conductive compared to other natural sediment compounds like silt, clay and organic matter (van Wijk and de Vries, 1966; de Vries, 1966). Based on the high thermal conductivity, calculated thermal diffusivity was also higher than diffusivities of natural streambed sediments (0.5×10^{-6} to $1 \times 10^{-6}\,m^2\,s^{-1}$). The calibrated baseline thermal conductivity of the saturated sediment was lower than the initial assumption based on volumetric averaging (arithmetic mean) of the thermal conductivities of water and quartz (Table 2). A much better estimate of the calibrated thermal conductivity has been derived by averaging the conductivity of water and quartz using the geometric mean (4.60 $W\,m^{-1}\,K^{-1}$). However, remaining deviations between calibrated and averaged hydraulic conductivities could be caused by the dependence of thermal conductivity upon the composition and arrangement of the solid phase.

3.5 Calculation of vertical water flow velocities based on amplitude ratios and time lags

Darcian flow velocities of the sand box experiment were calculated using the analytical solutions of the 1-D heat transport Eqs. (1) and (2). As input the amplitude ratios and time lags derived from the three setups (Sediment Probes, MLTS and combined PBS and PCS) and calibrated thermal parameter were used. Results of the shallow sensor pair$_{0.065\text{–}0.015}$ (Fig. 6) will be discussed in detail within this section. The result of the other sensors pairs are presented in Table (3) for brevity.

HESSD
8, 6155–6197, 2011

Flow velocities based on Sediment Probe amplitude ratios (v_{Sediment}) ranged from 1.75 to −0.75 m d^{-1} and revealed a high accordance with the measured fluxes (RMSE = 0.13 m d^{-1}, R^2 = 0.92) (Fig. 6a). The median of the normally distributed residuals between measured flow velocities and v_{Sediment} was only −0.025 m d^{-1} proving the appropriateness of the analytical solution based on Sediment Probes amplitude ratios.

Flow velocities based on MLTS derived amplitude ratios (v_{MLTS}) also highly agreed with the experimentally measured flow velocities (RMSE = 0.14 m d^{-1}, R^2 = 0.92) (Fig. 6a). The median of the residuals between measured flow velocities and v_{MLTS} was −0.046 m d^{-1}.

The results show that v_{Sediment} and v_{MLTS} were nearly identical, having low deviations for upward flow directions, arising from small differences in amplitude ratios between both setups (Sect. 3.3.1). In contrast, the vertical flow velocities based on PBS and PBC amplitude ratios ($v_{\mathrm{Piezometer}}$) highly differed from the measured flow velocities (RMSE = 0.48 m d^{-1}, R^2 = 0.39) (Fig. 6a). The median of the residuals between measured flow velocities and $v_{\mathrm{Piezometer}}$ was −0.33 m d^{-1} and the distribution of residuals were slightly skewed. Thus, the calculated flow velocities based on PBS and PCS amplitude ratios were generally higher than the measured ones. These deviations were due to thermal exchange processes within the piezometer pipes, which were not captured by the analytical solution. For experimental conditions, where differences of shallow and deep temperatures within the saturated sediment were small, $v_{\mathrm{Piezometer}}$ matched the measured flow velocities better. Such conditions mainly occurred during upward flow (days 63 to 83), when water influx at the bottom of the barrel caused homogeneous temperatures within the saturated sediment, while the penetration depth of the atmospheric temperature signal was small. During all other flow conditions, the vertical thermal exchange processes within the piezometer pipes highly affected the calculated flow velocities. Despite the general overestimation of $v_{\mathrm{Piezometer}}$, PBS and PCS amplitude ratios could be used to distinguish between upward, no and downward flow conditions, but they could not be reliably applied to determine flow velocity magnitudes.

HESSD
8, 6155–6197, 2011

The results of probe $\text{pair}_{0.165–0.065}$ and $\text{pair}_{0.365–0.165}$ reveal a decreasing agreement to measured fluxes with increasing probe spacing (Table 3). This decreasing accuracy was caused by variable temperatures at the bottom of the sand box during upward flow conditions. This temperature variability did affect sensors installed at 0.365 m more strongly than probes at 0.165 m and 0.065 m. For the downward flow condition, the accordance between measured and calculated flow velocities of all Sediment Probe and MLTS probe spacings was equal.

Vertical flow velocities derived from the time lag method highly differed from the measured flow velocities (Fig. 6b). The best fit was obtained for the Sediment Probe (RMSE = 0.78 m d^{-1}, R^2 = -0.67) and MLTS (RMSE = 0.87 m d^{-1}, $R^2 = -1.07$). Again, PBS and PCS showed the poorest fits (RMSE = 2.62 m d^{-1}, $R^2 = -16.57$). For all setups the time lag method was highly insensitive to small flow velocities and could not reflect measured flow velocities. Generally, the deviations between measured and calculated flow velocities of the Sediment Probe and MLTS decreased with increasing flux magnitude (Fig. 6b). Therefore, flow velocities accurately calculated by time lag method need to be higher than at least 1.5 m d^{-1}.

3.6 Sensitivity of calculated water flow velocities to sediment thermal properties and thermal dispersivity

The sensitivity analysis was based on the amplitude ratio method using the Sediment Probe $\text{pair}_{0.065–0.015}$. The calculated flow velocities (v_{Sediment}) were sensitive to variations of heat capacity and thermal conductivity, to simultaneous variations of heat capacity and thermal conductivity preserving the same thermal diffusivities, and to variations of temperature probe distance.

The de- and increase of heat capacity resulted in an absolute de- and increase of v_{Sediment}, respectively. Thereby v_{Sediment} was more sensitive to variations of the heat capacity during downward than during upward flow conditions (Fig. 7a). Under downward flow conditions, deep sediment temperatures were influenced by daily temperature variations. In contrast, deep sediment temperatures were homogeneous over time

HESSD
8, 6155–6197, 2011

during upward fluxes. Thus, less heat was absorbed and released by quartz grains than during downward fluxes, decreasing the solutions sensitivity to saturated heat capacity.

The calculated flow velocity was nearly insensitive to variations of thermal conductivity during downward flow conditions. For no-flow and upward flow conditions, a decrease of thermal conductivity caused higher and an increase of thermal conductivity caused lower estimates of v_{Sediment} (Fig. 7b). For upward flow conditions the direction of conduction is directly opposed to heat advection. The system was dominated by advection, however, the propagation of the thermal signal was determined by conduction through the sediment particles, increasing the solution's sensitivity to thermal conductivity.

As discussed for the optimisation of the thermal parameters, during no-flow conditions, calculated v_{Sediment} was insensitive to simultaneous changes of heat capacity and thermal conductivity as long as the thermal diffusivity remained unchanged. The simultaneous variations of both thermal properties yielded either an absolute underestimation (decreasing thermal properties) or an absolute overestimation (increasing thermal properties) of vertical flow velocity (Fig. 7c). These deviations were caused by the superposition of the described variations of v_{Sediment} for separated changes of heat capacity and thermal conductivity (Fig. 7a, b).

Absolute deviations of calculated flow velocities were highest for variations in temperature probe spacing (Fig. 7d). Therefore, a deviation of 50 % is unrealistic for probe distances higher than 5 cm, as it would decrease the solution's sensitivity, if probe distances were higher. Despite the exaggerated parameter ranges, experimental flow conditions were clearly distinguishable.

Sensitivity analyses of calculated v_{Sediment} revealed the need for an accurate estimation of thermal sediment properties and temperature probe spacing in order to accurately calculate vertical flow velocities. The omission of thermal dispersivity in the Keery et al.'s analytical solution of the 1-D heat transport equation (2007), might be a limitation when calculating vertical flow velocities. To test sensitivity of thermal

HESSD
8, 6155–6197, 2011

diffusivity to vertical flow velocity, the Hatch et al.'s solution (2006) was used (v_{Hatch}). The calculated flow velocities based on the Hatch amplitude ratio method were identical to the flow velocities calculated by Eq. (1), when the thermal diffusivity was set to zero. Also, v_{Hatch} results under consideration of thermal diffusivities in the range of solute dispersivity derived by conservative salt tracer experiment (Table 4) were similar to v_{Keery} (maximum deviation = 0.014 m d^{-1}, RMSE = 0.0015 m d^{-1}, R^2 = 0.99) with flow velocities ranging from −0.75 to 1.75 m d^{-1}. Therefore, the baseline thermal diffusivity (about 10^{-6} m^2 s^{-1}) was one order of magnitude higher than the maximal thermal dispersion coefficient (about 10^{-7} m^2 s^{-1}).

Our experimental results prove that the effect of thermal dispersion can be neglected for fine grained sediment and common water exchange fluxes between surface water and groundwater, when thermal dispersivity is equal to solute dispersivity.

4 Conclusions

Atmospheric temperature variations force the continuous transfer of energy between surface water and saturated sediment, thus forming subsurface temperature patterns determined by water flux direction and magnitude. The application of the analytical solution of the 1-D heat transport equation to observed temperature profiles provides a useful tool to quantify the water flux of saturated sediments. The accuracy of analytically calculated water fluxes was found to dependent on the temperature probe setup. Four temperature probe setups were installed into a sand box experiment to measure temporarily highly resolved vertical temperatures at depths of 0.015 m, 0.065 m, 0.165 m and 0.365 m under controlled exchange fluxes in the range of ±1.3 m d^{-1}.

Band pass filtering of the temperature records allowed extraction of the daily frequency, facilitating the use of analytical solutions to calculate vertical water flux. Amplitude ratios of the direct temperature probe installation setups 'Sediment Probes' and 'MLTS' significantly varied with sand box hydraulic gradients. These amplitude ratios provided an accurate basis for the analytical (amplitude ratio method) calculation of

Discussion Paper | Discussion Paper | Discussion Paper | Discussion Paper |
HESSD
8, 6155–6197, 2011
Influence of temperature probe design on vertical water flux calculation
M. Munz et al.
Title Page
Abstract Introduction
Conclusions References
Tables Figures
◀◀ ▶▶
◀ ▶
Back Close
Full Screen / Esc
Printer-friendly Version
Interactive Discussion

flow velocities in the range of $-1.29\,\mathrm{m\,d^{-1}}$ to $+0.75\,\mathrm{m\,d^{-1}}$. Best results were obtained for small temperature probe distances close to the surface-subsurface interface (probe $\mathrm{pair}_{0.065\text{–}0.015}$), guaranteeing that the shallow thermal regime is driven by atmospheric temperature oscillations and is independent of variable heat influx at the bottom of the sand box. Thermal properties of the medium-grained quartz sand were found to be $1870\,\mathrm{J\,kg^{-1}\,K^{-1}}$ for the heat capacity and $4.75\,\mathrm{W\,m^{-1}\,K^{-1}}$ for the thermal conductivity.

Calculated flow velocities were sensitive to thermal properties of the saturated sediment and to probe distance, but insensitive to thermal dispersivity equal to solute dispersivity. Measured temperature profiles of indirect temperature probe installations as PBS and PCS were disturbed by thermal exchange processes within the piezometer pipes. The thermal exchange, independently occurring from the saturated sediment, restricted the sensitivity of amplitude ratios to the sandbox hydraulic gradients and to the calculated water flow velocities.

Time lags of all temperature probe setups were generally insensitive to sand box hydraulic gradients, causing high deviations between measured and analytically (time lag method) calculated flow velocities in the range from $-1.29\,\mathrm{m\,d^{-1}}$ to $1.30\,\mathrm{m\,d^{-1}}$.

The interpretation of measured subsurface temperature data should contain a critical discussion of setup related effects, as thermal exchange processes within piezometer pipes are independent of saturated sediment. The representation of saturated sediment temperatures is of main importance for the accurate quantification of subsurface water fluxes.

The experimental results support that, besides the Sediment Probes, the MLTS setup can be used to accurately calculate vertical flow velocities. The advantage of MLTS is its installation into the saturated sediment, guaranteeing defined probe distances. The lost cone installation of Sediment Probes bears the potential to introduce deviations of defined temperature probe distances. The data of the MLTS setup can be accessed during operation by manually reading the logger or via the GSM modem. The temperature data of TidbiTs directly installed into the sediment can only be accessed after deinstallation. Data availability during operation enables the user to control the functioning of the setup and to promptly evaluate measurements. This prove the MLTS to be a valuable and appropriate tool for experimental application in natural streams to accurately quantify water and heat fluxes at the surface water-groundwater interface. The application along and across stream channels would provide highly resolved spatial and temporal information for better understanding the complex saturated sediment hydroecology.

References

Anderson, M. P.: Heat as a ground water tracer, Ground Water, 43, 951–968, 2005. 6157, 6167

Bear, J.: Dynamics of Fluids in Porous Media, Elsevier, New York, 1972. 6167, 6168

Boulton, A. J., Findlay, S., Marmonier, P., Stanley, E. H., and Valett, H. M.: The functional significance of the hyporheic zone in streams and rivers, Annu. Rev. Ecol. Syst., 29, 59–81, 1998. 6156

Bredehoeft, J. and Papadopolus: Rates Of Vertical Groundwater Movement Estimated From the Earth's Thermal Profile, Water Resour. Res., 1, 325–328, 1965. 6157

Cardenas, M. B.: Thermal skin effect of pipes in streambeds and its implications on groundwater flux estimation using diurnal temperature signals, Water Resour. Res., 46, W03536, doi:10.1029/2009WR008528, 2010. 6172

Carlslaw, H. S. and Jaeger, J. C.: Conduction of heat in solids, Clarendorn, Oxford, 2nd edn., 1959. 6188

Cirpka, O. A. and Kitanidis, P. K.: Characterization of mixing and dilution in heterogeneous aquifers by means of local temporal moments, Water Resour. Res., 36, 1221–1236, 2000. 6163

Cirpka, O. A. and Kitanidis, P. K.: Theoretical basis for the measurement of local transverse dispersion in isotropic porous media, Water Resour. Res., 37, 243–252, 2001. 6163

Conant, B.: Delineating and quantifying ground water discharge zones using streambed temperatures, Ground Water, 42, 243–257, 2004. 6168

Constantz, J.: Heat as a tracer to determine streambed water exchanges, Water Resour. Res., 44, W00D10, doi:10.1029/2008WR006996, 2008. 6157

Constantz, J. and Stonestrom, D. A.: Heat as a tracer of water movement near streams, U. S. Geological Survey, Circular 1260, 1–6, 2003. 6159

HESSD
8, 6155–6197, 2011

Influence of temperature probe design on vertical water flux calculation

M. Munz et al.

Constantz, J., Stonestrom, D., Stewart, A. E., Niswonger, R., and Smith, T. R.: Analysis of streambed temperatures in ephemeral channels to determine streamflow frequency and duration, Water Resour. Res., 37, 317–328, 2001. 6171

Constantz, J., Tyler, S. W., and Kwicklis, E.: Temperature-Profile Methods for Estimating Percolation Rates in Arid Environments, Vadose Zone Journal, 2, 12–24, 2003. 6157

de Marsily, G.: Quantitative Hydrogeology: Groundwater Hydrology for Engineers, Elsevier, New York, 1st edn., 1986. 6167

de Vries, D.: Thermal properties of soils, Physics of plant environment, North-Holland Publishing Co., Amsterdam, 2nd edn., 1966. 6177

Domenico, P. A. and Schwartz, F. W.: Physical and Chemical Hydrogeology, John Wiley and Sons Inc., New York, 2nd edn., 1990. 6161

Hatch, C. E., Fisher, A. T., Revenaugh, J. S., Constantz, J., and Ruehl, C.: Quantifying surface water-groundwater interactions using time series analysis of streambed thermal records: Method development, Water Resour. Res., 42, W10410, doi:10.1029/2005WR004787, 2006. 6157, 6158, 6159, 6160, 6167, 6168, 6170

Hopmans, J. W., Simunek, J., and Bristow, K. L.: Indirect estimation of soil thermal properties and water flux using heat pulse probe measurements: Geometry and dispersion effects, Water Resour. Res., 38, 1006, doi:10.1029/2000WR000071, 2002. 6167, 6177

Ingebritsen, S. E. and Sanford, W. E.: Groundwater in Geologic Processes, Cambridge Univ. Press, New York, 1998. 6167

Jensen, J. K. and Engesgaard, P.: Nonuniform Groundwater Discharge across a Streambed: Heat as a Tracer, Vadose Zone Journal, 10, 98–109, 2011. 6157

Kalbus, E., Reinstorf, F., and Schirmer, M.: Measuring methods for groundwater – surface water interactions: a review, Hydrol. Earth Syst. Sci., 10, 873–887, doi:10.5194/hess-10-873-2006, 2006. 6156

Keery, J., Binley, A., Crook, N., and Smith, J. W. N.: Temporal and spatial variability of groundwater-surface water fluxes: Development and application of an analytical method using temperature time series, J. Hydrol., 336, 1–16, 2007. 6157, 6158, 6159, 6167, 6168, 6171

Krause, S., Hannah, D. M., Fleckenstein, J. H., Heppell, C. M., Kaeser, D., Pickup, R., Pinay, G., Robertson, A. L., and Wood, P. J.: Inter disciplinary perspectives on processes in the hyporheic zone, Ecohydrology, 4, 2011. 6156

Lapwood, E. R.: Convection Of A Fluid In A Porous Medium, Proceedings Of The Cambridge

Philosophical Society, 44, 508–521, 1948. 6168
Lautz, L. K.: Impacts of nonideal field conditions on vertical water velocity estimates from streambed temperature time series, Water Resour. Res., 46, W01509, doi:10.1029/2009WR007917, 2010. 6157
Rau, G. C., Andersen, M. S., McCallum, A. M., and Acworth, R. I.: Analytical methods that use natural heat as a tracer to quantify surface water-groundwater exchange, evaluated using field temperature records, Hydrogeol. J., 18, 1093–1110, 2010. 6157, 6159
Rosenberry, D. O. and LaBaugh, J. W.: Field Techniques for Estimating Water Fluxes Between Surface Water and Ground Water, U. S. Geological Survey, Techniques and Methods 4-D2, 2008. 6156
Schmidt, C., Bayer-Raich, M., and Schirmer, M.: Characterization of spatial heterogeneity of groundwater-stream water interactions using multiple depth streambed temperature measurements at the reach scale, Hydrol. Earth Syst. Sci., 10, 849–859, doi:10.5194/hess-10-849-2006, 2006. 6157
Schmidt, C., Conant, B., Bayer-Raich, M., and Schirmer, M.: Evaluation and field-scale application of an analytical method to quantify groundwater discharge using mapped streambed temperatures, J. Hydrol., 347, 292–307, 2007. 6157
Schön, J.: Physical Properties of Rocks: Fundamentals and Principles of Petrophysiks, Porgamon, Oxford, 2nd edn., 1998. 6177
Schornberg, C., Schmidt, C., Kalbus, E., and Fleckenstein, J. H.: Simulating the effects of geologic heterogeneity and transient boundary conditions on streambed temperatures – Implications for temperature-based water flux calculations, Adv. Water Resour., 33, 1309, doi:10.1016/j.advwatres.2010.04.007, 2010. 6157
Silliman, S. E., Ramirez, J., and McCabe, R. L.: Quantifying Downflow Through Creek Sediments Using Temperature Time-Series – One-Dimensional Solution Incorporating Measured Surface-Temperature, J. Hydrol., 167, 99–119, 1995. 6157
Sinokrot, B. A. and Stefan, H. G.: Stream temperature dynamics: Measurements and modeling, Water Resour. Res., 29, 2299–2312, doi:10.1029/93WR00540, 1993. 6158
Sophocleous, M.: Interactions between groundwater and surface water: the state of the science, Hydrogeol. J., 10, 52–67, 2002. 6156
Stallman, R. W.: Steady 1-Dimensional Fluid Flow In A Semi-Infinite Porous Medium With Sinusoidal Surface Temperature, J. Geophys. Res., 70, 2821, doi:10.1029/JZ070i012p02821, 1965. 6157, 6159

Stonestrom, D. A. and Blasch, K. W.: Determining temperature and thermal properties for heat-based studies of surface-water ground-water interactions, U. S. Geological Survey, Circular 1260, 73–80, 2003. 6166, 6177

Suzuki, S.: Percolation Measurements Based On Heat Flow Through Soil With Special Reference To Paddy Fields, J. Geophys. Res., 65, 2883–2885, 1960. 6157

Turcotte, D. L. and Schubert, G.: Geodynamics: Application of Continuum Physics to Geologic Problems, John Wiley and Sons, New York, 1982. 6157

van Wijk, W. and de Vries, D.: Periodic temperature variations in a homogeneous soil. In Physics of plant environment, North-Holland Publishing Co., Amsterdam, 2nd edn., 1966. 6177, 6188

Wierenga, P. J., Nielsen, D. R., and Hagan, R. M.: Thermal Properties Of A Soil Based Upon Field And Laboratory Measurements, Soil Sci. Soc. Am. Pro., 33, 354–360, 1969. 6166

HESSD

8, 6155–6197, 2011

Influence of temperature probe design on vertical water flux calculation

M. Munz et al.

Table 1. Defined hydraulic head differences (Δh) of sand box experiment, averaged gradient dependent fluxes at system outlet ($\overline{q}$) with corresponding deviations of 95 % confidence intervals to $\overline{q}$, period length of constant hydraulic gradient and calculated Peclet and Rayleigh numbers of each Δh condition.

Δh (m)	$\overline{q}$ ($m^3 m^{-2} d^{-1}$)	Deviation of 95% confidence intervals to $\overline{q}$ ($m^3 m^{-2} d^{-1}$)	Period length (d)	Peclet number	Rayleigh number
−0.026	1.30	±0.04	12	14.3	0.78
−0.013	0.69	±0.02	9	7.6	2.05
−0.008	0.53	±0.10	12	5.8	2.61
−0.002	0.19	±0.03	11	2.1	6.02
0	–	–	18	0	6.95
0.002	−0.25	±0.07	9	2.8	5.74
0.008	−0.48	±0.06	11	5.3	7.03
0.013	−0.67	±0.03	7	7.4	3.61
0.026	−1.29	±0.16	7	14.2	4.37

HESSD
8, 6155–6197, 2011

Table 2. Thermal properties of sand box individual phases -water, quartz and HDPE- and of saturated porous media.

	Density ($kg\,m^{-3}$)	Heat capacity ($J\,kg^{-1}\,K^{-1}$)	Volumetric heat capacity ($J\,m^{-3}\,K^{-1}$)	Thermal conductivity ($W\,m^{-1}\,K^{-1}$)	Thermal diffusivity ($m^2\,s^{-1}$)
Water	1000[a]	4182[a]	4182000	0.60[a]	1.43×10^{-7}
Quartz	2700[b]	733[b]	1900000	8.40[b]	4.20×10^{-6}
Saturated sediment	2140	1870	4000000	5.44	2.69×10^{-6}
HDPE[c]	–	–	2137500	0.49	2.42×10^{-4}

[a] Carlslaw and Jaeger (1959)
[b] van Wijk and de Vries (1966)
[c] www.matbase.com/material/polymers/commodity/hdpe/properties

HESSD
8, 6155–6197, 2011

Table 3. Comparison of measured and calculated Darcian flow velocities based on Sediment Probes, MLTS and Piezometer Probe amplitude ratios and different temperature probe spacings.

	RMSE (m d^{-1})			R^2		
	Sediment Probes	MLTS	Piezometer Probes	Sediment Probes	MLTS	Piezometer Probes
Probe Pair$_{0.065-0.015}$	0.13	0.14	0.48	0.92	0.92	0.39
Probe pair$_{0.165-0.065}$	0.21	0.19	0.52	0.88	0.90	0.28
Probe pair$_{0.365-0.015}$	0.35	0.30	0.62	0.68	0.74	−0.05

HESSD

8, 6155–6197, 2011

Influence of temperature probe design on vertical water flux calculation

M. Munz et al.

Table 4. Sand box characteristics and sediment hydraulic properties.

Parameter	Value
Sandbox surface area (A)	$0.350\,m^2$
Total porosity (n)	0.370
Effective porosity (n_e)	0.330
Saturated hydraulic conductivity (K_{sat})	$2.24 \times 10^{-4}\,m\,s^{-1}$
Dispersion coefficient (D_{Disp})	$1.5 \times 10^{-7}\,m^2 s^{-1}$
Longitudinal dispersivity (α)	0.013 m

HESSD
8, 6155–6197, 2011

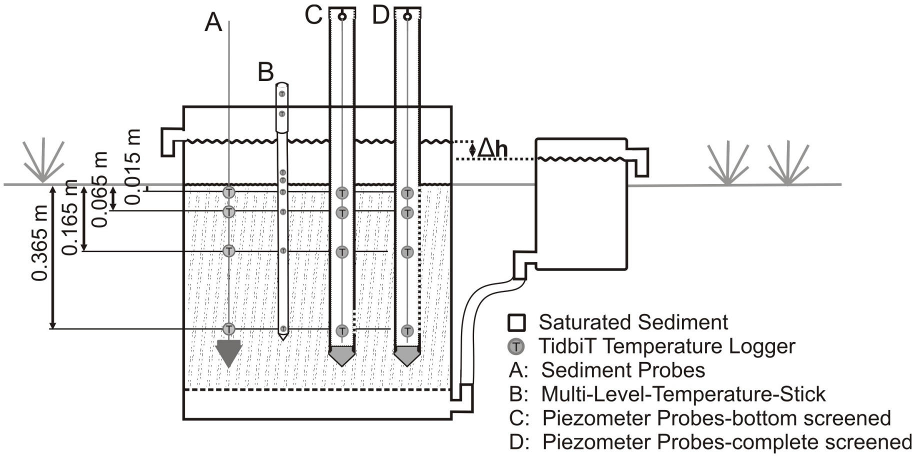

Fig. 1. Experimental setup of sand box experiment and of temperature probe installations **(A–D)** with temperature loggers at various depths (0.015 m–0.365 m) below ground surface.

HESSD
8, 6155–6197, 2011

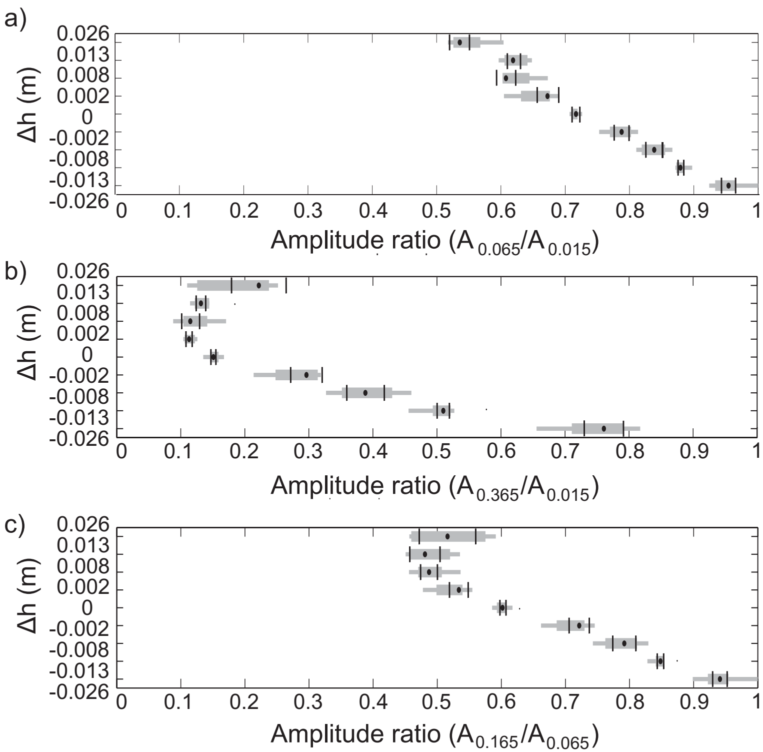

Fig. 2. Daily amplitude ratio distribution of Sediment Probe pairs 0.065–0.015 **(a)**, 0.365–0.015 **(b)** and 0.165–0.065 **(c)** of all sand box hydraulic head differences. Data distribution of each condition is shown by box plot (gray shape) with median value of daily amplitude ratios (black dot) and the corresponding 95 % confidence intervals of median value (black mark). Note that a negative hydraulic head difference indicates water flux in vertical downward direction.

HESSD
8, 6155–6197, 2011

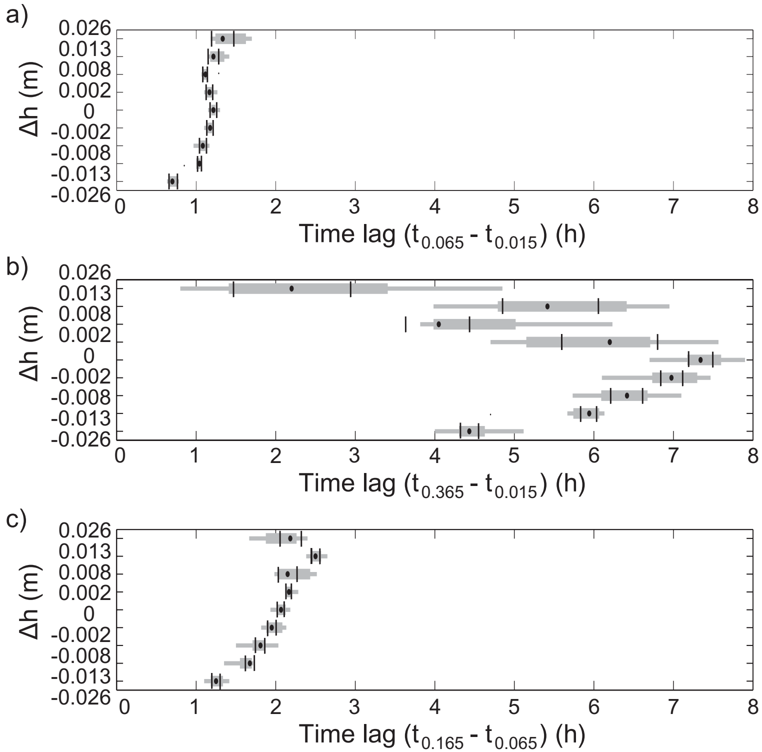

Fig. 3. Daily time lag distribution of Sediment Probe pairs 0.065–0.015 **(a)**, 0.365–0.015 **(b)** and 0.165–0.065 **(c)** of all sand box hydraulic head differences. Data distribution of each condition is shown by box plot (gray shape) with median value of daily amplitude ratios (black dot) and the corresponding 95 % confidence intervals of median value (black mark). Note that a negative hydraulic head difference indicates water flux in vertical downward direction.

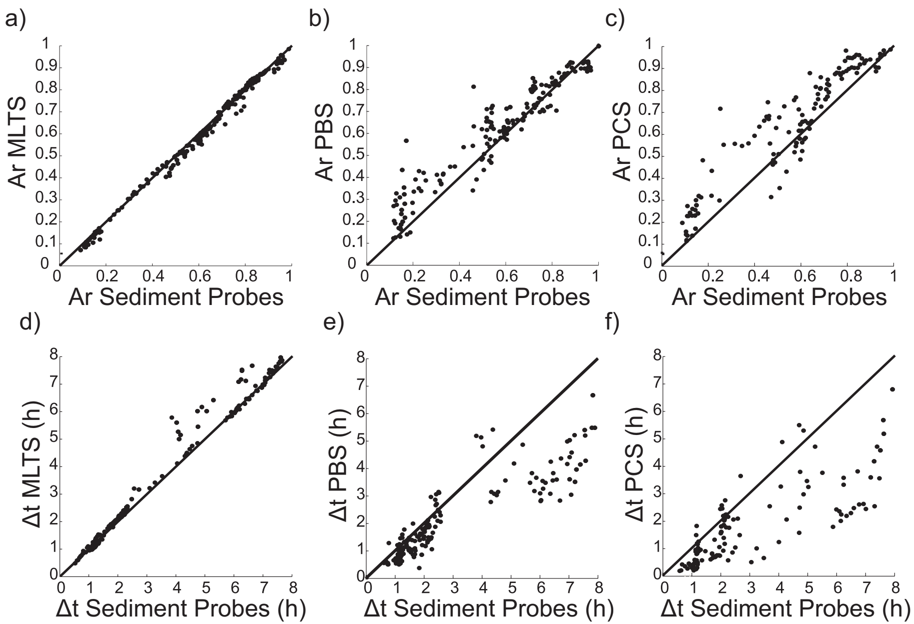

Fig. 4. Scatter plots of amplitude ratio of Sediment Probes vs. amplitude ratio of Multi Level Temperature Stick **(a)**, bottom screened Piezometer Probes **(b)** and complete screened Piezometer Probes **(c)** and scatter plots of time lag of Sediment Probes vs. time lag of MLTS **(d)**, bottom screened Piezometer Probes **(e)** and complete screened Piezometer Probes **(f)** of all daily ratios of probe pairs 0.065–0.015, 0.365–0.015 and 0.165–0.065. The diagonal line is the 1:1 line.

HESSD
8, 6155–6197, 2011

Influence of temperature probe design on vertical water flux calculation

M. Munz et al.

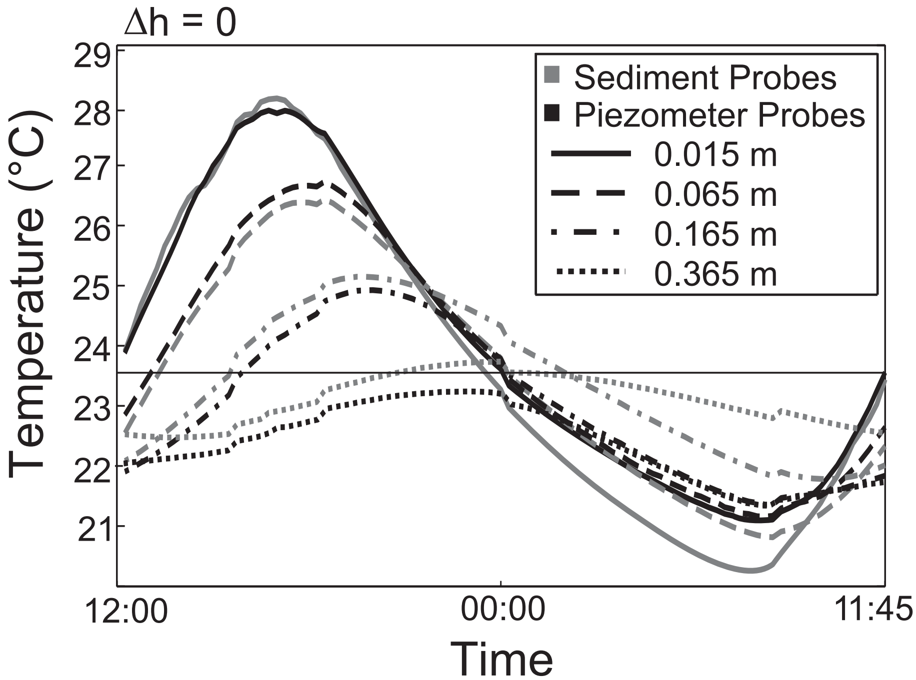

Fig. 5. Measured average daily temperature cycle of the Sediment and bottom screened Piezometer Probes of no flow condition ($\Delta h = 0$).

HESSD
8, 6155–6197, 2011

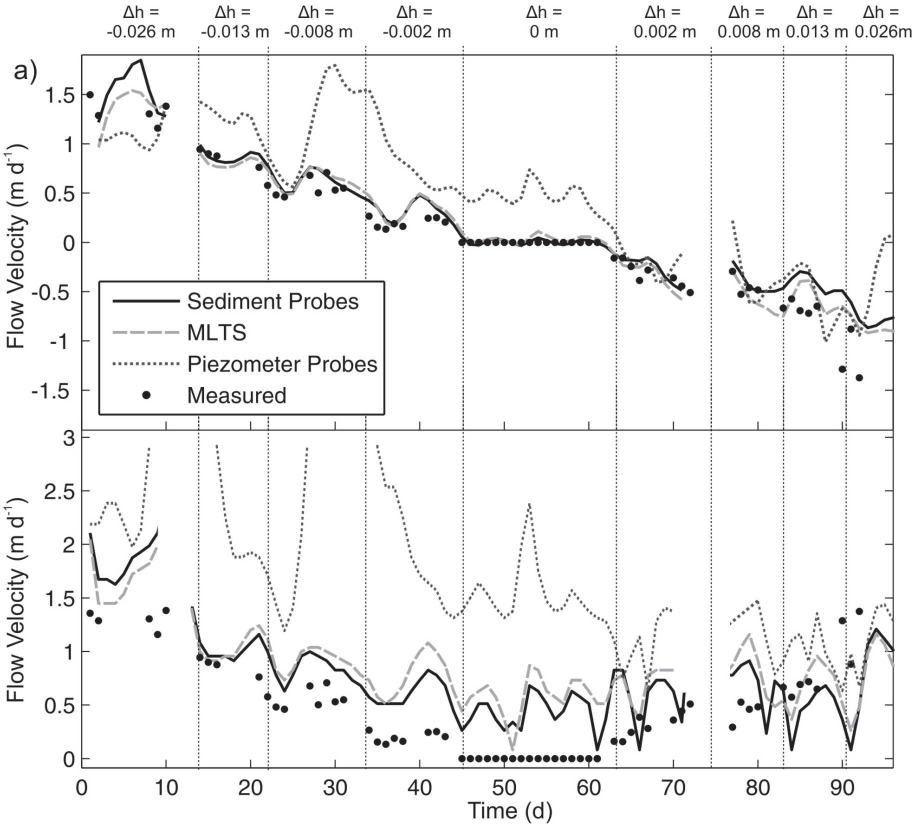

Fig. 6. Calculated Darcian flow velocities of sand box experiment using Keery's amplitude ratio **(a)** and time lag method **(b)**. Amplitude ratios and time lags were derived by temperature time series evaluation of Sediment Probe pair$_{0.065-0.015}$.

HESSD

8, 6155–6197, 2011

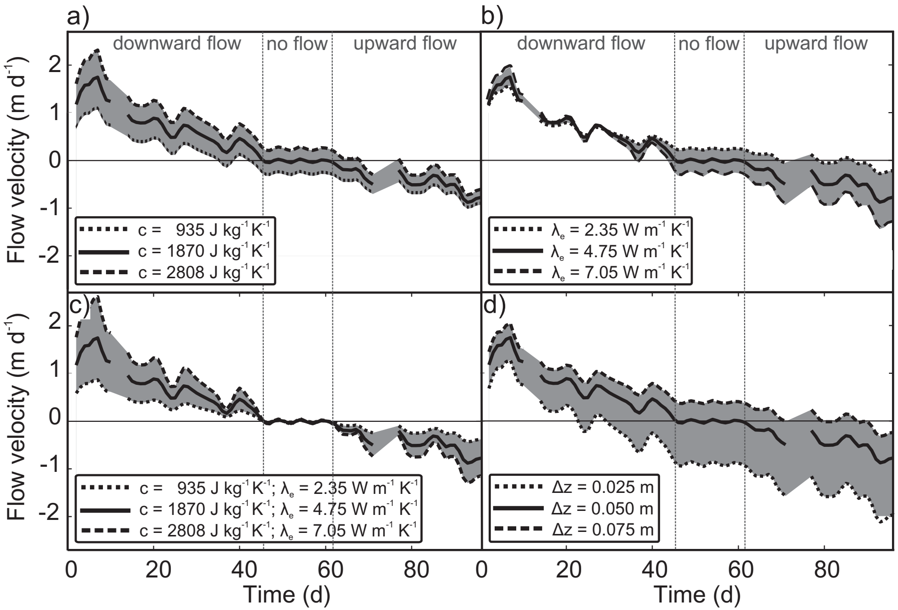

Fig. 7. Sensitivity of analytically calculated Darcian flow velocities to variations of heat capacity **(a)** and thermal conductivity **(b)**, to simultaneous variations of heat capacity and thermal conductivity guaranteeing same thermal diffusivities **(c)** and to variations of temperature probe spacing **(d)**.

HESSD
8, 6155–6197, 2011